

Received:
23 May 2018
Revised:
4 August 2018
Accepted:
13 September 2018

Cite as: N. Shaari,
S. K. Kamarudin,
S. Basri. Molecular dynamics
simulations of sodium
alginate/sulfonated graphene
oxide membranes properties.
Heliyon 4 (2018) e00808.
doi: [10.1016/j.heliyon.2018.e00808](https://doi.org/10.1016/j.heliyon.2018.e00808)



Molecular dynamics simulations of sodium alginate/sulfonated graphene oxide membranes properties

N. Shaari^{a,*}, S. K. Kamarudin^{a,b,**}, S. Basri^a

^a *Fuel Cell Institute, Universiti Kebangsaan Malaysia, 43600 UKM Bangi, Selangor, Malaysia*

^b *Chemical Engineering Programme, Faculty of Engineering and Built Environment, Universiti Kebangsaan Malaysia, 43600 UKM Bangi, Selangor, Malaysia*

* Corresponding author.

** Corresponding author.

E-mail addresses: norazuwanashaari@ukm.edu.my (N. Shaari), ctie@ukm.edu.my (S.K. Kamarudin).

Abstract

The influence of methanol as a solvent on the properties of sodium alginate/sulfonated graphene oxide (SA/SGO) membranes was explored in water-methanol mixed conditions with various methanol concentrations and temperatures through molecular dynamics simulations. The methanol uptake of the membrane showed an isolation phase determined from the simulation results. The distance between the sulfonic acid groups increased in higher methanol concentrations, as observed from S-S RDFs. Furthermore, the distance between the SA-chain RDFs and the solvent molecules was analysed to determine a) the affinity of water towards the sulfonic acid groups and b) the affinity of the aromatic backbone of the SA towards methanol molecules. A decrease in water molecule diffusion led to an increase in methanol diffusion and uptake. SA/SGO membranes exhibited a smaller diffusion coefficient than that for the Nafion membranes, as calculated from simulation results and compared to the experimental work. Additionally, the diffusion ability increased at higher temperatures for all permeants. The interaction information obtained is useful for DMFC applications.

Keywords: Chemical engineering, Materials chemistry, Materials science

1. Introduction

Direct methanol fuel cells are mainly used in portable and stationary applications, and they have attracted the attention of many researchers in recent years. Proton electrolyte membranes (PEMs) are the heart of this system, and they function as a separator between the anode and cathode, an inhibitor for fuel crossover and a pathway for proton [1, 2]. Nafion is the most favourable PEM due to its high stability and conducting properties, but it is still limited by its high methanol crossover, which leads to low selectivity (ratio of the proton conductivity to the methanol permeability) [3]. However, many researchers have been unable to find safe alternative membranes that show better or similar performance compared to that of Nafion while reducing costs. The polymer electrolyte membrane performance is usually evaluated by the ion conductivity, water uptake capability and fuel permeability. There are many works focusing on the development of new polymeric membranes to replace Nafion membranes, such as SPEEK, PBI, PVA, and SPPO as well as biopolymers such as alginate- and chitosan-based membranes [2, 4, 5, 6]. The sodium alginate biopolymer has a monomer structure, as shown in Fig. 1.

Research on sodium alginate as a membrane, especially in DMFCs, is limited, but it has been widely applied in various fields, including packaging, medical tools and membranes. However, this polymer has several weaknesses, such as excess hydrophilicity, low mechanical stability, and low proton conductivity. As reported by Pardini Cabello et al. [7], the proton conductivity of an alginate carrageenan membrane was 9.8 mS cm^{-1} . The advantages of the sodium alginate polymer in terms of low cost, abundance and environmental friendliness cannot be denied. Thus, the other materials can be part of a sodium alginate-based membrane to reduce the drawbacks, as previous studies have reported [8, 9, 10, 11, 12, 13, 14]. Molecular level studies have been implemented on biopolymer types such as chitosan, as carried out by LópezChávez et al. [15] and Srinophakun & Martkumchan [16], who reported that the ionic conductivity of a chitosan membrane was $2 \times 10^{-2} \text{ S cm}^{-1}$ and $7.14 \times 10^{-2} \text{ S cm}^{-1}$, respectively, using a COMPASS force field [17]. In addition, the modelling studies for polymers other than biopolymers were also implemented using the same method with poly(ethylene oxide) sulfonic acid anions, PVF-based polyelectrolyte, Dow, Nafion and Aciplex membranes to find the mechanism of the ionic activity [18, 19]. Vishnyakov & Neimark [20] and Mahajan & Ganesan [21] ran

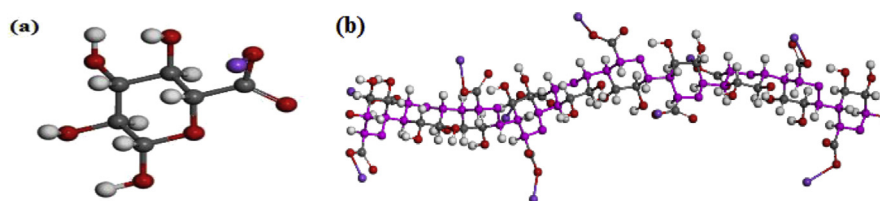


Fig. 1. Structural representation of the (a) monomer unit, (b) and polymer chain of sodium alginate.

simulations to observe the influence of the methanol solution on the Nafion and SPEEK membrane. In other hand, the activated carbon structure has been predicted through molecular dynamic simulation [22].

Based on our knowledge, there are no studies to date on sodium alginate using a molecular dynamics modelling simulation. This study aims to determine the ionic conductivity, water uptake capability and methanol permeability in different methanol concentrations in the presence of hydronium ions. An amorphous cell builder is used to construct a system containing alginate, sulfonated graphene oxide, hydronium ions, water molecules and methanol. The COMPASS force field was applied to run the molecular modelling system. The output result from the modelling simulation can be used to determine the interaction, diffusivity and ion conductivity and, thus, can predict the overall ion mechanism activity in the system. The methanol concentration was varied from 0, 20, 40, 60, and 80 wt% with various temperatures.

2. Methods

2.1. Atomistic models and amorphous cell construction

The COMPASS force field was set and applied in Accelrys commercial software (Materials Studio 7.0) to construct polymer membrane systems and their simulation studies. The membrane system was built using an amorphous cell builder with a construction task followed by a minimization process to get the minimum energy using the Forcite module. The water molecule, hydronium ion, methanol and SGO were drawn and then minimized by the steepest descent and conjugate gradient method in the discovery module. The sodium alginate monomer was drawn using a 3D-atomistic molecule; then, polyalginate was constructed through the polymer builder module with 10 repeating units of the alginate monomer and 5 chains followed by a minimization step. Next, the polyalginate, SGO, hydronium, methanol and water molecules were constructed in an amorphous cell box with periodic boundary conditions. The amount of water and methanol were varied to see their effects on the polyalginate/SGO system, as presented in Table 1. The five different systems consisted of five chains of polyalginate with 10 repeating units, 20 hydronium ions, 4 sheets of SGO, 5 glycerol molecules and 0, 20, 40, 60 or 80 wt% methanol under DMFC conditions.

Three different temperature settings were applied, namely, 298, 320, and 340 K, to study the effect of temperature on the membrane interaction. The distribution of various water amounts near the polyalginate membrane can be seen in Fig. 2 as it is assumed to be similar to the real system in DMFC. Minimization steps were applied on the amorphous system to achieve 0.1 kcal/mol for its maximum derivative. An optimum sulfonation of 27% determined by Hasani-Sadrabadi et al. [23] was used to set the sulfonation of SGO, which was considered 25%. The minimized

Table 1. Composition of SA/SGO membranes used for MD simulations and cell sizes for methanol concentrations of 0, 20, 40, 60 and 80 wt%.

System	1	2	3	4	5
Methanol concentration, wt%	0	20	40	60	80
Sodium alginate	5	5	5	5	5
SGO	4	4	4	4	4
Hydronium	20	20	20	20	20
Water	200	160	120	80	40
Methanol	0	40	80	120	160
Glycerol	5	5	5	5	5
Density (g cm ⁻³)	1.4217	1.4258	1.3749	1.3887	1.3674
Cell volume (Å ³)	20545	21832	23318	23757	24809

SGO structure contained 24 benzene rings, of which 5 were sulfonated at a 25% sulfonation degree. Theoretically, the sulfonic acid functional groups were completely ionized; thus, they can be the indicator of the hydronium ion number, which is equal to the number of sulfonic acid groups, in an attempt to keep the simulation cells in a neutral condition. Dissociated protons from the water molecules create the hydronium ions, as reported in a previous work that studied hydrated PEMS [21, 24, 25, 26, 27, 28]. The five simulation cells were running with a constant number of solvent molecules (CH₃OH + H₂O), which referred to the number of water molecules, with a water content of $\lambda = 9$ (λ , is the ratio of the number of water molecules to the fixed number of sulfonic acid groups). The initial density was set at a very low value of 0.005 g cm³ for all 3-D amorphous cell simulations of the SA/SGO membrane and final density achieved is higher as shown in Fig. 3. The initial process of cell construction was determined to be at a certain density in order to avoid problems with ring catenation attributed to the presence of an alginate aromatic backbone, allowing for faster simulation cell equilibration.

2.2. MD simulations

The amorphous simulation cells must achieve an equilibrium condition particularly for the composite aromatic structure, which is of significant concern. Thus, the annealing and minimization step on the SA/SGO polymeric membrane structure has been applied with the same method used for previous work with Nafion, SPEEK, SPPO membrane simulations [20, 27, 29]. A smart minimizer has been applied to eliminate any close links among all the atoms and for preliminary relaxation. Three steps exist in the MD simulations, which are as follows: 1) NVT-MD simulation: the sampling time step and long dynamics runs were 1.0 fs and 200 ps at 298 K to free the system from any potential tension. The sampling time step was set due to the previous work by Srinophakun & Martkumchan [16] which has been work out on chitosan membrane for PEM fuel cell. 2) NPT-MD simulations at a pressure = 1 bar

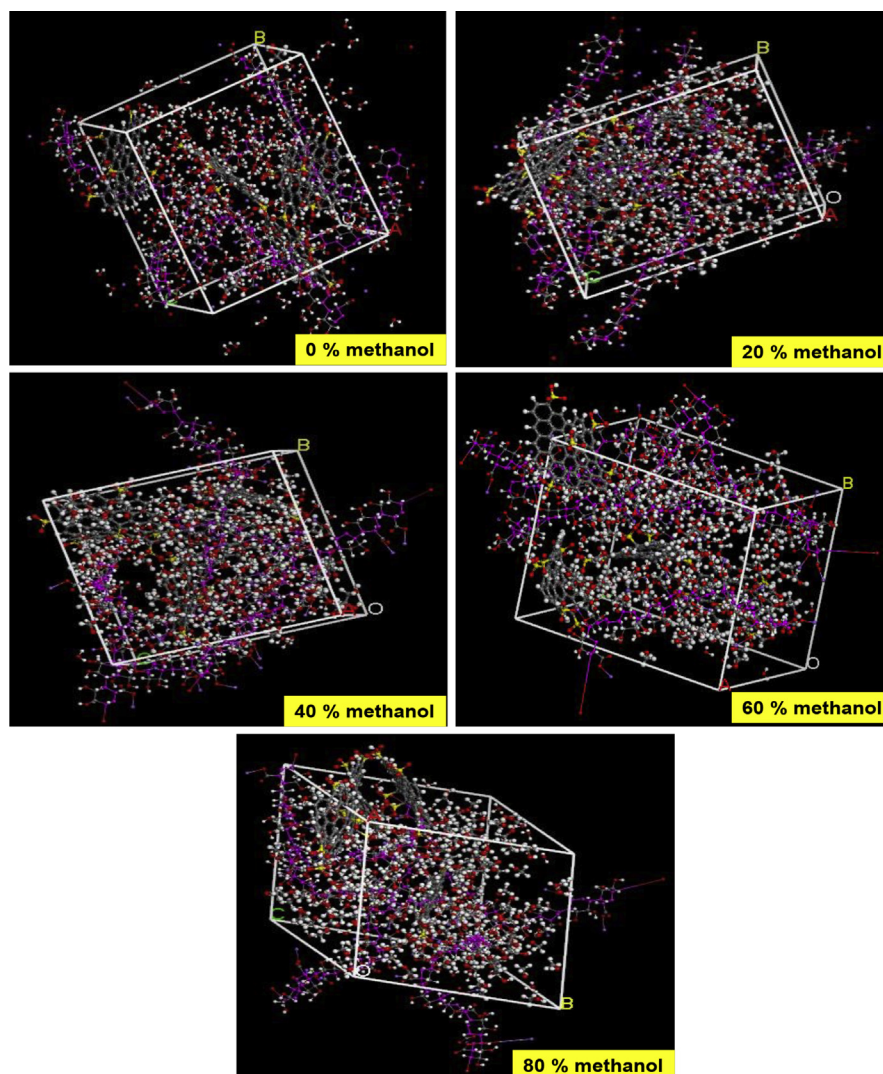


Fig. 2. Final snapshots of water-methanol solvated SA/SGO membranes for 0, 20, 40, 60 and 80 wt% methanol concentrations obtained at the end of production phase MD simulations. For all membranes the color code is: polymeric chains backbone: grey; water oxygen, hydronium ion oxygen, sulfonic acid oxygen and methanol oxygen atoms: red; sulfur atoms: yellow; water hydrogen, hydronium ion hydrogen and methanol hydroxyl hydrogen atoms: white and methanol methyl groups (CH₃): green.

and a temperature = 298 K, which run until they reach equilibrium state, depending on the atomic number in the system. This step initiates changes in the shape and size of the amorphous cell to reach an equilibrium density for all molecular structures. The density profile presented in Fig. 4 was recorded throughout the NPT-MD simulation. 3) NVT-MD simulation: The sampling time step and long dynamics runs were 1.0 fs and 200 ps at 298 K for previous equilibrated systems. The Andersen thermostat and barostat were chosen as the temperature regulator. The Ewald summation method was applied to measure the van der Waals and coulombic non-

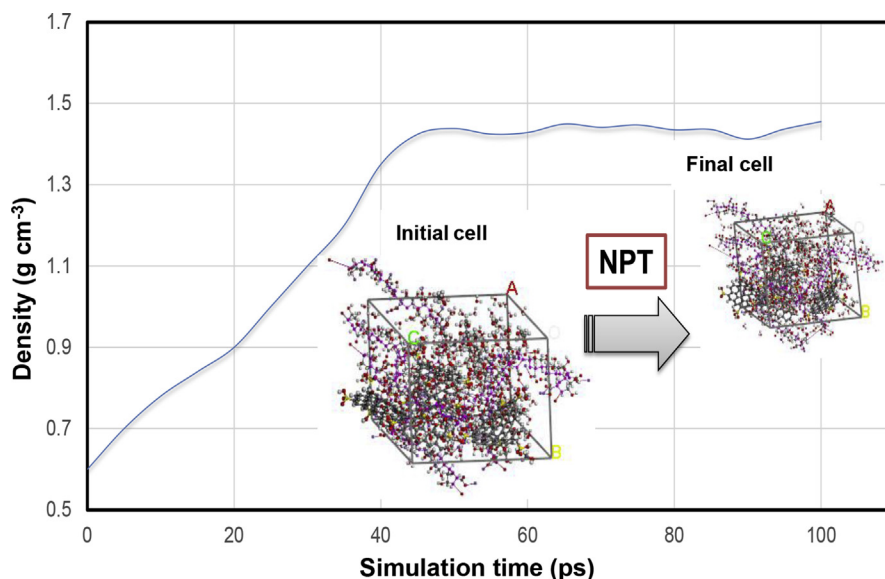


Fig. 3. The time evolution density profiles during NPT–MD simulation of SA/SGO system. The density of system was changed from 0.6 to 1.289 g·cm⁻³, and the NPT–MD simulation time was 200 ps. After NPT–MD simulation, the specification of final cell becomes smaller than the initial.

bonding interactions. The mean square displacement (MSD) was measured from a molecular dynamics study run, and the diffusion coefficient and ion conductivity were obtained. The Eq. (1.0) below was used to determine the diffusivity, D .

$$D = \frac{1}{6N} \lim_{t \rightarrow \infty} \frac{d}{dt} \rightarrow \infty \frac{1}{N} \sum_{i=1}^N [R_i(t) - R_i(0)]^2 \quad (1.0)$$

The MSD is the result of N divided by the sum term on the right-hand side of Eq. (1.0). N refers to the diffusing particles number, t is time, and $R_i(t)$ is the particles vector location at time event t . This equation is applicable if Einstein diffusion is applied, which explains that the diffusing particle movement is random; in other

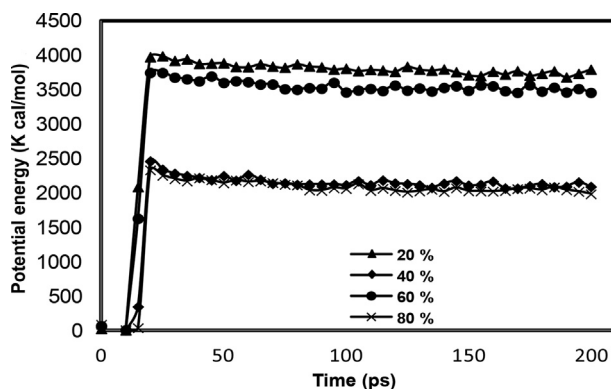


Fig. 4. Variation of total potential energy of the amorphous simulation systems with different methanol concentrations during 200 ps production phase MD simulations.

words, the movement of diffusing particles at time t is independent of the movement at any prior time. The Einstein equation was applied to determine the ionic conductivity of each system, as in Eq. (2.0) [18, 30].

$$\sigma = \frac{Nz^2e^2D}{VkT} \quad (2.0)$$

where σ is the ionic conductivity, e is the elemental charge, V is volume of the simulation cell, k is the Boltzmann constant, T is temperature, and z is the total charge in units of e .

The hydronium ion and water molecule allocation in the system was analysed in reference to the intermolecular correlation function, denoted by $g(r)$ in the computational step. The intermolecular pair correlation function, $g(r)$, corresponds to the possibility of the discovery of a pair of particles, A . . . B, at a certain distance (r) normalized according to the possibility estimated for the total allocation at an equivalent arbitrary density, and it is defined according to Eq. (3.0)

$$g_{A-B} = \frac{\frac{n_B}{4\pi r^2 \Delta r}}{\frac{N_B}{V}} \quad (3.0)$$

where n_B is the number of atoms located around A atoms inside a spherical shell of thickness Δr , and N_B is the total number of B atoms applied for an amorphous cell.

Fig. 4 displays the unchanged total potential energy of all simulation cells because their oscillations are considered small throughout the 200 ps dynamics simulation time, which can be an indicator that the system reached an equilibrium condition.

3. Results & discussion

The results from the computational simulations will be evaluated in this part, which covers the findings of the molecular interactions, ionic conductivity and ion transfer mechanism.

3.1. Static property analysis

Table 1 lists the volume, density and number of particles of each cell with different concentrations of methanol. The sulfur-sulfur interaction in the sulfonic acid group has been determined by the RDF graph, as shown in Fig. 5, with various methanol concentrations for the SA/SGO solvated membrane system.

Fig. 5 shows the S–S RDFs, which have an initial peak at 1.55 Å and a second peak at 2.47 Å under different hydration and methanol levels. There was local aggregation but not electrostatic repulsion in the S-S pair [31]. The intensity of the first peak increased with increasing methanol concentration and decreasing water content,

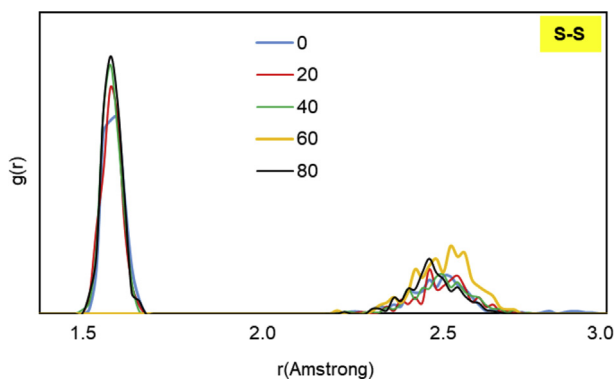


Fig. 5. RDFs of sulphur-sulphur atomic pair of sulfonic acid group for different methanol concentrations at 298 K.

showing that the sulfur atom interactions with each other increase when the methanol concentration increases, which is due to the swelling of the membrane with channel expansion and the disruption from the aggregation of sulfonate groups.

The sulfur atom RDFs towards oxygen and methyl groups in the methanol molecule are presented in Fig. 6a and b, respectively, in different methanol concentrations. The first peak of the S-Om and S-Cm RDFs appeared at 1.55 Å and 1.09 Å, correspondingly. It is observed that the intensity of the RDF peak for S-Om and S-Cm increased with the increase in the methanol concentration. As the content in the

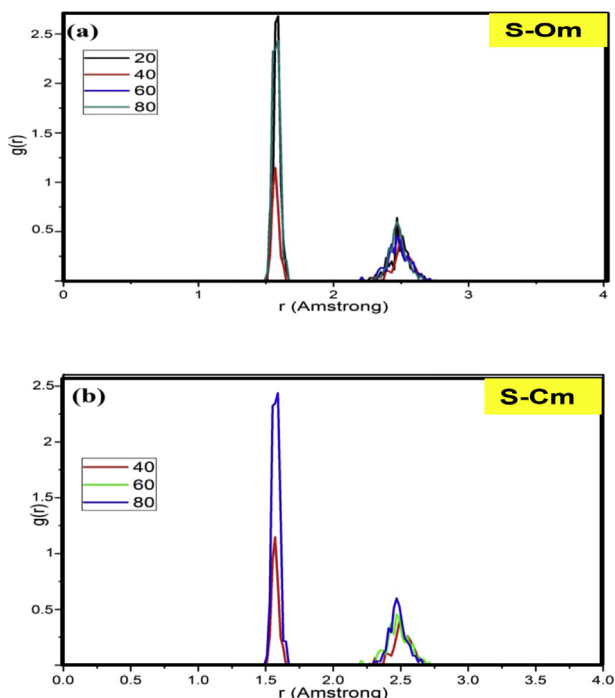


Fig. 6. (a) RDF for Sulphur (sulfonic acid group) - oxygen (methanol), (b) sulphur (sulfonic acid group) - methyl (methanol).

methanol molecular system increased, the number of water molecules declined, thus leading to higher methanol uptake by the membrane due to a decreased selection effect of water on the methanol molecules. Fig. 7a and b shows the RDF graph for the Os-Om and Os-Cm RDFs, respectively. The prominent peak with the highest intensity occurred at 2.41–2.57 Å for the Os-Om RDFs and 1.07 Å for the Os-Cm RDFs, respectively, for different methanol concentrations, which present the same development as the RDF of that of S-Om and S-Cm.

The RDF of the sulfonic group towards the methanol molecule has a high intensity due to interactions between the hydrogen atom in the hydroxyl group of methanol and the oxygen atom in the sulfonic group, which form a hydrogen bond. This is also caused by the anionic sulfonic acid groups surrounded by a high number of methanol molecules. Hence, the separation of the SGO nanosheets phase can indirectly be induced by the presence of methanol molecules. A higher methanol concentration shows a greater influence of methanol on the sulfonic acid groups.

The RDF graph of the sulfur atoms of the sulfonic acid groups towards the oxygen atoms of the water (Ow) and hydronium ion (Oh) are presented in Fig. 8(a) and (b), respectively. The RDF S-Ow had a prominent peak at 1.57 Å for 0% and 20% and at 1.53 Å for a 40%, 60%, and 80% methanol concentration. In the case of RDF S-Oh, the highest peak appeared at 1.57 Å for 0% and 20% and at 1.55 Å for a 40%, 60%

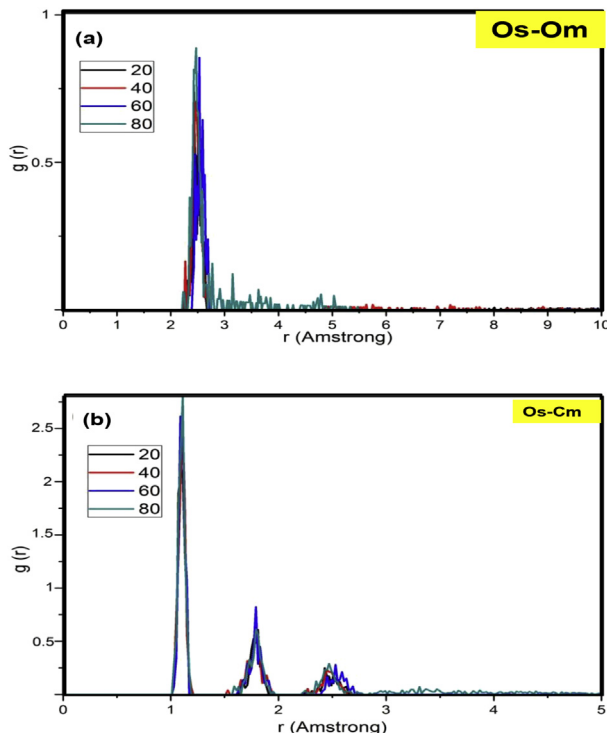


Fig. 7. (a) oxygen (sulfonic acid group) – oxygen (methanol) and (b) oxygen (sulfonic acid group) –methyl (methanol) for different methanol concentrations at 298 K.

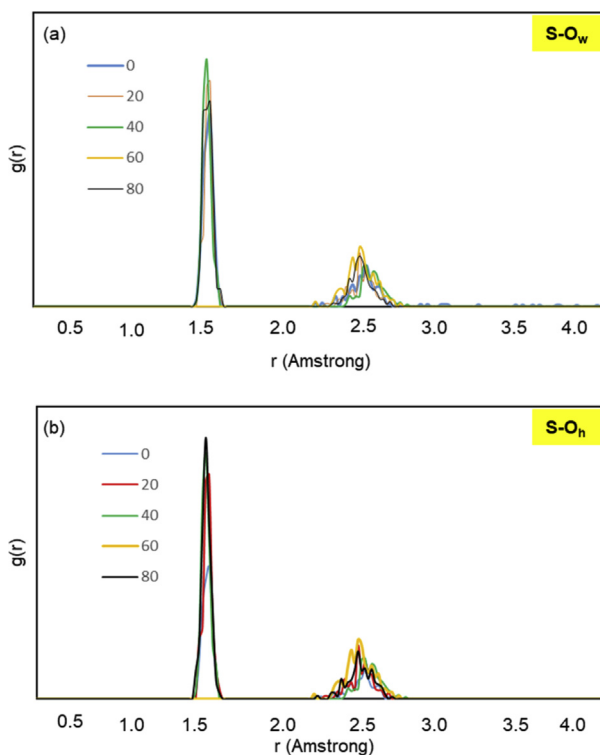


Fig. 8. RDFs of (a) sulfur (sulfonic acid group) - oxygen (water) and (b) sulfur (sulfonic acid group) - oxygen (hydronium ion) for different methanol concentrations at 298 K.

and 80% methanol concentration. As the methanol concentration increased, the RDF peak height also increased for both cases, RDF S-O_w and RDF S-O_h, which was attributed to a diminished water solvent selection effect on water and hydronium ions under high methanol concentrations. The intensity of the S-O_w RDFs was observed to be higher than that of S-O_m RDFs from the previous part (Fig. 6a); it can be said that the water molecule had greater attraction towards the sulfonic acid groups than the methanol molecule in the membrane system containing a water-methanol mixed solvent, which is due to a decrease in the effect of the water solvent on hydronium ions, thus maintaining the position of the hydronium ions, which are close to the sulfonic acid groups.

In summary, from the observed sulfonic acid group peak in the RDFs with respect to the methanol, water and hydronium ion peaks, it is inferred that the SA/SGO membranes in an aqueous solution of methanol as the solvent demonstrated a phase-separated microstructure consisting of hydrophilic (ionic) and hydrophobic regions, which was also observed in our recent MD simulation studies of pure SPEEK [32], SPPO [24], and SPEEK-SPES [26] membranes in water as a solvent. This observation is consistent with the experimental results for alcohol solvated perfluorinated membranes reported by Saito et al. [33].

The interaction between the carbon backbones of the sodium alginate polymer with the solvent oxygen atoms was also observed in various methanol concentrations. According to Fig. 9a, the RDFs of C-O_w have a high intensity that is higher than unity from 20 wt% to 80 wt% methanol. However, the increase in the methanol concentration shows a small reduction in the intensity of the interaction between the carbon backbone and the water oxygen molecule. When the methanol concentration increased, the carbon was attracted to the methanol molecule, but the amount of water remained high around the carbon backbone, which is attributed to the hydrophilic nature of the sodium alginate polymer.

Fig. 9b shows the RDFs of C-O_m, which also have intensities higher than unity. The interaction of the carbon backbone towards the oxygen in methanol increases when the methanol concentration increases due to the higher amount of methanol that surrounds the carbon backbone at higher methanol concentrations. This refers to the LJ interactions of the backbone carbon of the sodium alginate chains with a methanol methyl group [34]. The water molecule exhibits strong attraction towards both the sulfonic acid groups and the carbon backbone of the sodium alginate polymer.

The interaction between the hydronium ion and the oxygen atoms of the water and methanol molecules was observed from the RDF plots, as presented in Fig. 10a and

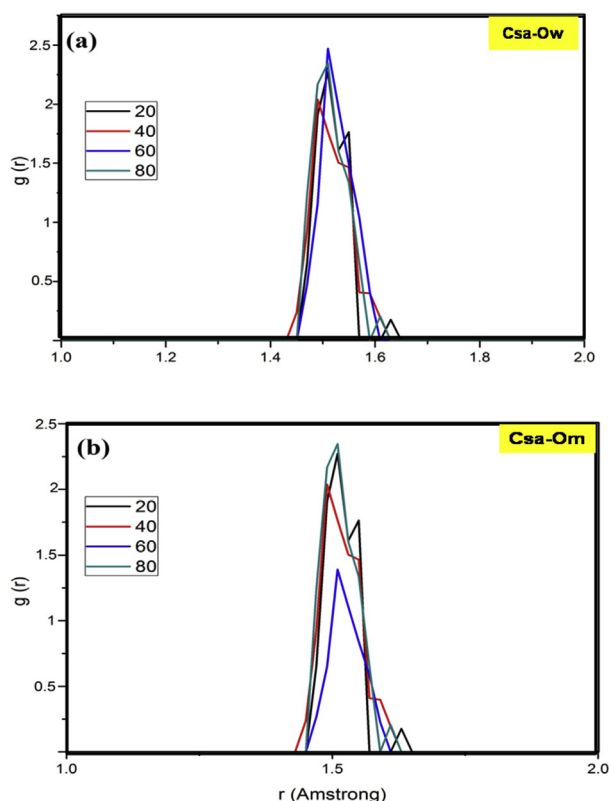


Fig. 9. RDFs of (a) aromatic carbon (backbone)- oxygen (water) and (b) aromatic carbon (backbone) – oxygen (methanol) for different methanol concentrations at 298 K.

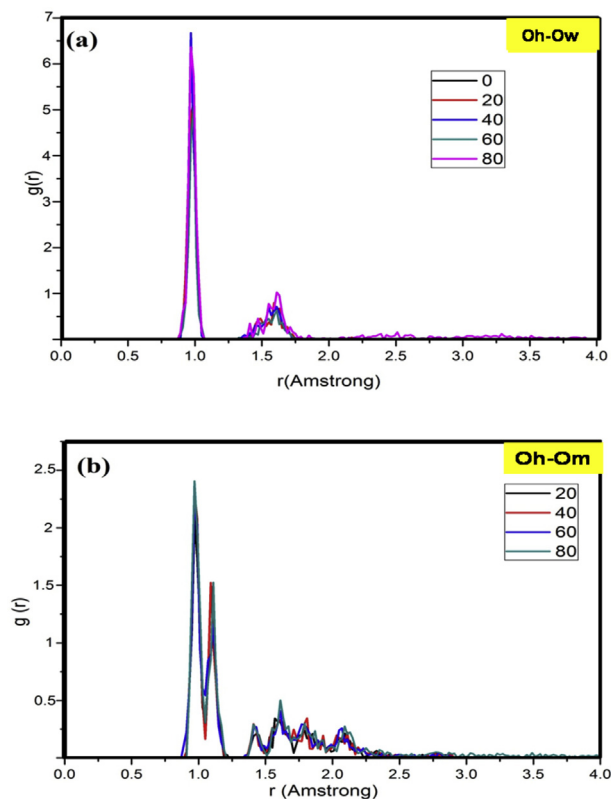


Fig. 10. RDFs of (a) oxygen (hydronium ion) – oxygen (water) and (b) oxygen (hydronium ion) – oxygen (methanol) for different methanol concentrations at 298 K.

b, under different methanol concentrations. The prime peak occurred at a 0.95 \AA radius, which is very similar in both cases and shows a similar trend in the intensity with the increase in the methanol concentration. This is mainly caused by a reduction in the water selection effect at high methanol concentrations. It is obvious that the RDF for Oh-Ow has a higher intensity than Oh-Om, which can be determined because the number of water molecules around the hydronium ions is much greater than the number of methanol molecules in the system of an SA/SGO membrane solvated by a water-methanol solvent.

The RDFs of a water oxygen to another water oxygen is exhibited in Fig. 11(a) (Ow-Ow). The prominent peak was located at 0.97 \AA for all concentrations of methanol. The intensity was increased from 0-40 wt% methanol, and the results show that oxygen atoms in water have a strong interaction with each other in this methanol concentration range. However, at 60 wt% methanol, the water screening effect becomes weaker towards water oxygen due to the increase of methanol molecules inside the system. However, the intensity increased again at 80 wt% methanol, which indicates the formation of water clusters inside the system at very high methanol concentrations.

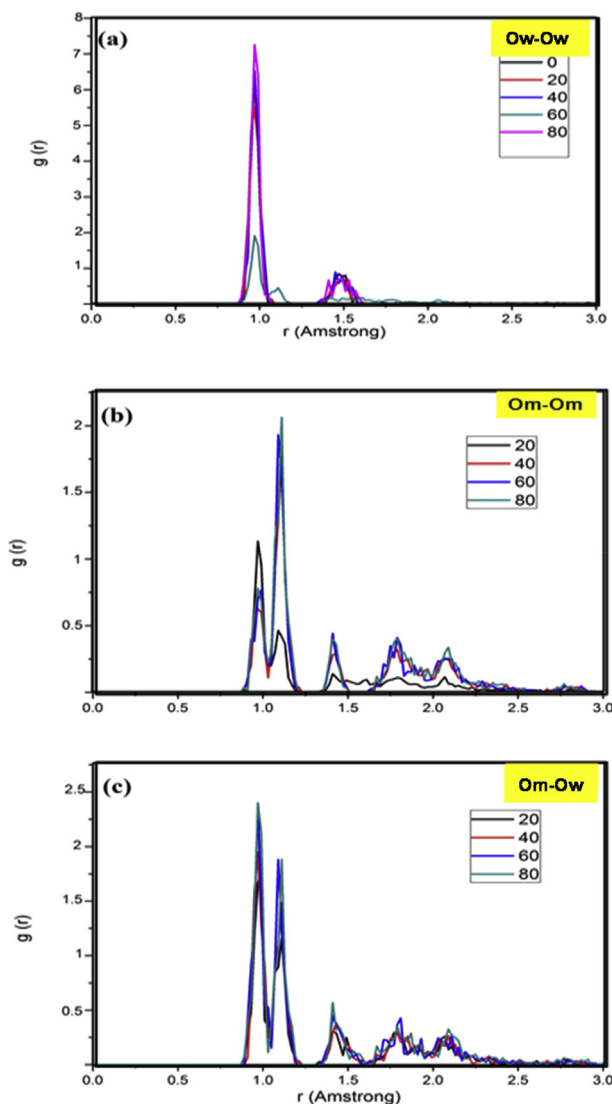


Fig. 11. RDFs of (a) oxygen (water) – oxygen (water), (b) oxygen (methanol) - oxygen (methanol) and (c) oxygen (methanol) – oxygen (water); for different methanol concentrations at 298 K.

Fig. 11(b) and (c) revealed the RDF plots of the oxygen atoms in the methanol solvent towards methanol oxygen (Om-Om) and water oxygen atoms (Om-Ow) for various methanol concentrations. The pronounced peak of the RDFs of Om-Om and Om-Ow appear at 1.09 Å and 0.97 Å, respectively. Both graphs have a similar increasing trend for the intensity with increasing methanol concentrations. In the case of the RDFs of Om-Om, the number of methanol oxygen atoms interacting with methanol oxygen atoms increases at higher concentrations due to an increasing number of methanol molecules in the system. Meanwhile, for the Om-Ow RDF plot, the methanol molecule has a high capability in cluster formation even with another molecule known as solvent cluster due to the aggregation phenomena. Solvent clusters can be roughly observed by viewing the membrane solvated system in Fig. 2.

Conversely, when the methanol concentration increased, the number of methanol molecules located near the methanol solvents increased. A separation phase occurred inside the solvated SA/SGO membrane system due to the formation of solvent clusters involving water and methanol solvents, as presented by the RDFs in Fig. 11.

3.2. Dynamics property analysis

The diffusion ability of the hydronium ion, water molecules and methanol molecules can be evaluated in the SA/SGO membrane solvated system and, thus, can elaborate on their dynamical properties. The diffusion coefficient was a quantitative indicator. To determine the temperature effect on the diffusion calculation in the membrane system, 40 wt% methanol was considered.

The MSD curves for the hydronium ion and water in various methanol concentrations at 298 K are presented in Fig. 12a and b. The MSD curves were approximately linear for both the hydronium and water permeants, indicating that the movement of permeants in the SA/SGO membrane was constant. Fig. 12(c) present the MSD of hydronium ion in 40 wt% methanol at different temperature.

Fig. 13(a) provides the simulated diffusion coefficients of the hydronium ion, water and methanol for the varied concentrations of methanol, while Fig. 13(b) shows them with respect to the temperature variation. The water diffusivity increased when the methanol concentration increased from 0-60 wt% but slightly decreased when the methanol concentration increased up to 80 wt%, which is related to a decrease in the size of the water molecule clusters in 80 wt% methanol. For the methanol molecule diffusion, the trend decreased when the methanol concentration increased, which might be due to the higher number of methanol molecules that formed solvent clusters, inhibiting the diffusion of methanol molecules in the system. The 20 wt% methanol system produces a high methanol diffusion coefficient, and from this, we can assume that 20 wt% is the optimum methanol concentration. The high methanol concentration used in the DMFC single cell test can also decrease the performance up to a certain concentration; thus, the proper concentration must be selected [35]. The hydronium ions, methanol and water seem most active in the system with 20 wt% methanol. The diffusion of hydronium ions calculated in this simulation only considers the vehicular mechanism without including the Grotthuss mechanism, and therefore, it is not an exact condition. The decrease in the hydronium ion diffusion at higher methanol concentrations is caused by the low number of ions compared to the methanol and solvent cluster formation, which also inhibits the movement of hydronium ions in the system. Fig. 13(b) shows the diffusion coefficient for all permeants at different temperatures. Methanol and water molecules have higher diffusion rates at higher temperatures, which relates to the effect of heat on the molecule vibration and movement. However, hydronium ions show a reduction in diffusion rate at higher temperatures. The mobility of the hydronium

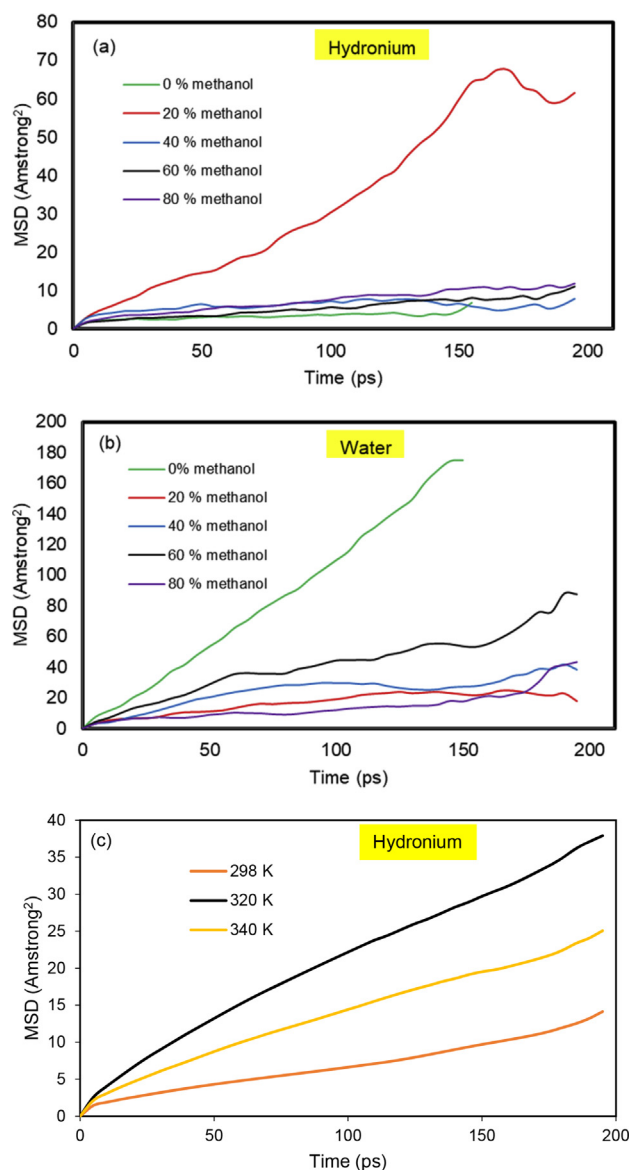


Fig. 12. MSD of (a) hydronium ions, (b) water molecules and inside the water-methanol at different methanol concentrations at 298 K (c) hydronium ion in 40 wt% methanol at different temperature.

ions may be hindered by the active movement of the methanol and water molecules. However, the calculation of the hydronium ion diffusion in this simulation is not the same as the real diffusion, which involves both the Grotthuss and vehicular mechanisms.

Previous studies by Vishnyakov & Neimark [20] have also studied the effect of methanol concentration in water-methanol solvents but with developed Nafion membranes. The methanol diffusion coefficient in this study was 5.145×10^{-11} , 2.22×10^{-11} , 1.169×10^{-12} , and 1.709×10^{-12} for methanol concentrations of 20%, 40%, 60% and 80%, respectively. The methanol diffusion coefficient in the water-

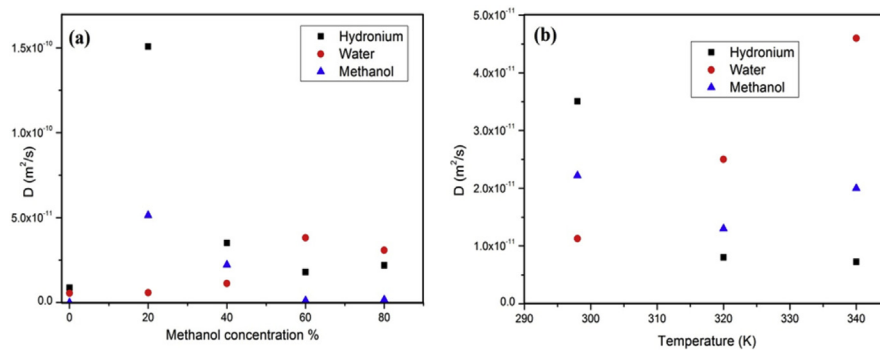


Fig. 13. Diffusion coefficients of hydronium ions, water molecules and methanol molecules (a) in SA/SGO membranes for different methanol concentrations at 298 K and (b) in SA/SGO membranes with 40 wt% methanol concentration at different temperatures.

methanol dissolved SPPO membrane was 0.0032 , 0.0033 , 0.0057 and $0.0072 \times 10^{-8} \text{ m}^2 \text{ s}^{-1}$, respectively, for 20%, 40%, 60% and 80% methanol concentrations, respectively. Chen et al. [27] reported that the diffusion coefficients for methanol were 0.0829 , 0.0898 and $0.0993 \times 10^{-8} \text{ m}^2 \text{ s}^{-1}$ for methanol concentrations of 11.23%, 21.40% and 46.92% at 323 K, respectively.

This comparison shows that the methanol diffusion rate in this study is lower than that of other studies, which can be attributed to the low methanol permeability properties of the developed SA/SGO biomembranes. The results of the methanol permeability tests in the experimental work was recorded in our previous study, which $1.535 \times 10^{-7} \text{ cm}^2 \text{ s}^{-1}$ was the lowest permeability of methanol for SA/SGO membrane. According to the actual study of Nafion and SPPO membranes Hasani-Sadradadi et al. [23], the permeability values of methanol are 2×10^{-6} and 1.7×10^{-7} , respectively. This value gives a good indication of the SA/SGO membrane developed with a low methanol permeability either from the experimental or simulation results.

Table 2 lists the simulated diffusion coefficients of the methanol, water and hydronium ions in various methanol and temperature systems with different ionic conductivities. From the calculation of the ionic conductivity, only the diffusion coefficient of the hydronium ion is considered. The value of the ionic conductivity in the 20% methanol system is the highest compared to that of the other systems. From 0% to 20% methanol, the ionic conductivity increased due to water absorption, and the hydronium ions were at optimum levels, while the methanol was not present in excess amounts.

However, the ionic conductivity decreased in the 40%–80% methanol concentrations. This reduction may be due to the effect of the high methanol barrier on the movement of hydronium ions and the occurrence of methanol in the membranes, which decreased the membrane performance [36]. The ionic movement mechanisms

Table 2. Diffusion coefficient ($\text{m}^2 \text{s}^{-1}$) for methanol molecule, water molecule and hydronium ion in different methanol concentration system at 298 K.

System	Temperature (K)	Methanol molecule	Water molecule	Hydronium ion	Conductivity ion ($\times 10^{-3}$) S cm^{-1}
0 wt%	298	0	5.53×10^{-12}	8.775×10^{-12}	4.95
20 wt%	298	5.145×10^{-11}	5.83×10^{-12}	1.508×10^{-10}	8.61
40 wt%	298	2.22×10^{-11}	1.126×10^{-11}	3.51×10^{-11}	18.8
60 wt%	298	1.169×10^{-12}	3.814×10^{-11}	1.795×10^{-11}	9.41
80 wt%	298	1.709×10^{-12}	3.08×10^{-11}	2.189×10^{-11}	100.2

in the simulation consider only the transport mechanism (vehicular), while the jumping mechanism (hopping or Grotthuss) is excluded in the estimation. Therefore, the transport mechanism is limited due to the increase in the amount of methanol, which causes some hydronium ion movement.

Additionally, as the methanol concentration increases, the amount of water molecules decreases. Water is a transport agent or vehicle in the proton scans, and this is also a major factor contributing to a decrease in the ionic conductivity in higher methanol concentrations. The values in this simulation are not accurate because the resulting system is not the same as the actual membrane state. There are many things that are not considered in the simulation, such as an approximation of the methanol pathway, the jumping mechanism and so forth. However, this simulation can provide a rough guideline of the interactions that are expected to occur in the membrane.

4. Conclusion

Classical MD simulation techniques were applied to investigate the effects of methanol solvent on various properties of polymeric membranes based on SA materials solvated with five different methanol concentrations: 0, 20, 40, 60 and 80 wt%. The transport of hydronium ions, water and methanol within the membrane was also examined at different temperatures of 320 and 340 K. The simulation results exhibited phase segregation behaviour in SA/SGO membranes with the uptake of methanol solvent molecules. To examine the distribution of hydronium ions, water and methanol inside the membrane and their relationship with respect to the sulfonic acid groups and aromatic backbone of SA materials RDF analysis was performed. From evaluation of the S-S RDFs, it was found that with increasing methanol concentration, the average distance between neighbouring hydrophilic sulfonic acid groups increased. A comparison of the solvation ability of the solvent molecules for sulfonic acid groups and backbone of SA showed that the sulfonic acid groups

were surrounded by more water molecules than methanol molecules, while the aromatic backbone of SA was found to be hydrophobic and showed a greater affinity towards methanol. The hydronium ion RDFs with water and methanol solvents suggested stronger solvation of hydronium ions with water molecules than with methanol. Additionally, the RDFs for water and methanol demonstrated the clustering of solvents. The diffusion coefficient of the water molecules within the SA/SGO membrane decreased as the methanol concentration increased, while those of the methanol solvents increased. A slight variation in diffusion coefficient of hydronium ions versus the methanol concentration existed. Furthermore, the diffusivity for all permeants enhanced as the temperature increased except for hydronium ions. The calculated methanol diffusion coefficients in the SA/SGO membranes were smaller than the reported values in the Nafion membrane, which indicated a reduction in transport of methanol in the SA/SGO membranes compared to that in Nafion and solvated pure SPPO membranes because of their desirable features, such as the phase-separated microstructure, and the formation of solvent clusters and a slower methanol transport property, and as a result, the SA/SGO membranes can be considered a candidate PEMs for use in DMFCs.

Declarations

Author contribution statement

Norazuwana Shaari: Performed the experiments; Analyzed and interpreted the data; Contributed reagents, materials, analysis tools or data; Wrote the paper.

Siti Kartom Kamarudin: Analyzed and interpreted the data; Contributed reagents, materials, analysis tools or data.

Sahriah Basri: Analyzed and interpreted the data; Contributed reagents, materials, analysis tools or data; Wrote the paper.

Funding statement

This work was supported by the Universiti Kebangsaan Malaysia (UKM) under DPP-2018-003.

Competing interest statement

The authors declare no conflict of interest.

Additional information

No additional information is available for this paper.

Acknowledgements

We are very thankful to the reviewers and editor for providing valuable suggestions to improve the manuscript, we also thank our lab mates who encouraged us to carry out this work.

References

- [1] N. Shaari, S.K. Kamarudin, Chitosan and alginate types of bio-membrane in fuel cell application: an overview, *J. Power Sources* 289 (2015) 71–80.
- [2] H. Ahmad, et al., A novel hybrid Nafion-PBI-ZP membrane for direct methanol fuel cells, *Int. J. Hydrogen Energy* 36 (22) (2011) 14668–14677.
- [3] Z. Zakaria, S.K. Kamarudin, S.N. Timmiati, Membranes for direct ethanol fuel cells: an overview, *Appl. Energy* 163 (2016) 334–342.
- [4] B.G. Kim, et al., LbL assembled sPPO composite membrane containing GO for DMFC applications, *Mol. Cryst. Liq. Cryst.* 598 (1) (2014) 16–22.
- [5] G. Rambabu, S.D. Bhat, Sulfonated fullerene in SPEEK matrix and its impact on the membrane electrolyte properties in direct methanol fuel cells, *Electrochim. Acta* 176 (2015) 657–669.
- [6] M. Buraidah, A. Arof, Characterization of chitosan/PVA blended electrolyte doped with NH₄ I, *J. Non-Cryst. Solids* 357 (16) (2011) 3261–3266.
- [7] S.D. Pasini Cabello, et al., New bio-polymeric membranes composed of alginate-carrageenan to be applied as polymer electrolyte membranes for DMFC, *J. Power Sources* 265 (2014) 345–355.
- [8] Y. He, et al., Alginate/graphene oxide fibers with enhanced mechanical strength prepared by wet spinning, *Carbohydr. Polym.* 88 (3) (2012) 1100–1108.
- [9] M. Ionita, M.A. Pandeale, H. Iovu, Sodium alginate/graphene oxide composite films with enhanced thermal and mechanical properties, *Carbohydr. Polym.* 94 (1) (2013) 339–344.
- [10] PaÅÿcalÄfu, V., et al., The alginate/k-carrageenan ratio's influence on the properties of the cross-linked composite films. *J. Alloy. Comp.* 536, Suppl. 1: p. S418-S423.
- [11] M.A.d. Silva, A.a.C.K. Bierhalz, T.G. Kieckbusch, Alginate and pectin composite films crosslinked with Ca²⁺ ions: effect of the plasticizer concentration, *Carbohydr. Polym.* 77 (4) (2009) 736–742.

- [12] B. Smitha, S. Sridhar, A.A. Khan, Chitosan–sodium alginate polyion complexes as fuel cell membranes, *Eur. Polym. J.* 41 (8) (2005) 1859–1866.
- [13] E. Tavassoli-Kafrani, H. Shekarchizadeh, M. Masoudpour-Behabadi, Development of edible films and coatings from alginates and carrageenans, *Carbohydr. Polym.* 137 (2016) 360–374.
- [14] A.K. Vipin, S. Ling, B. Fugetsu, Sodium cobalt hexacyanoferrate encapsulated in alginate vesicle with CNT for both cesium and strontium removal, *Carbohydr. Polym.* 111 (2014) 477–484.
- [15] E. López-Chávez, et al., Molecular modeling and simulation of ion-conductivity in chitosan membranes, *Polymer* 46 (18) (2005) 7519–7527.
- [16] T. Srinophakun, S. Martkumchan, Ionic conductivity in a chitosan membrane for a PEM fuel cell using molecular dynamics simulation, *Carbohydr. Polym.* 88 (1) (2012) 194–200.
- [17] H. Sun, COMPASS: an ab initio force-field optimized for condensed-phase applications overview with details on alkane and benzene compounds, *J. Phys. Chem. B* 102 (38) (1998) 7338–7364.
- [18] J. Ennari, Modelling of transport properties and state of water of polyelectrolytes containing various amounts of water, *Polymer* 49 (9) (2008) 2373–2380.
- [19] C. Zheng, F. Geng, Z. Rao, Proton mobility and thermal conductivities of fuel cell polymer membranes: molecular dynamics simulation, *Comput. Mater. Sci.* 132 (2017) 55–61.
- [20] A. Vishnyakov, A.V. Neimark, Molecular dynamics simulation of nafion oligomer solvation in equimolar Methanol– water mixture, *J. Phys. Chem. B* 105 (32) (2001) 7830–7834.
- [21] C.V. Mahajan, V. Ganesan, Atomistic simulations of structure of solvated sulfonated poly (ether ether ketone) membranes and their comparisons to Nafion: I. Nanophase segregation and hydrophilic domains, *J. Phys. Chem. B* 114 (25) (2010) 8357–8366.
- [22] P.-Y. Yang, S.-P. Ju, S.-M. Huang, Predicted structural and mechanical properties of activated carbon by molecular simulation, *Comput. Mater. Sci.* 143 (2018) 43–54.
- [23] M.M. Hasani-Sadrabadi, S.H. Emami, H. Moaddel, Preparation and characterization of nanocomposite membranes made of poly (2, 6-dimethyl-1, 4-phenylene oxide) and montmorillonite for direct methanol fuel cells, *J. Power Sources* 183 (2) (2008) 551–556.

- [24] G. Bahlakeh, M. Nikazar, Molecular dynamics simulation analysis of hydration effects on microstructure and transport dynamics in sulfonated poly (2, 6-dimethyl-1, 4-phenylene oxide) fuel cell membranes, *Int. J. Hydrogen Energy* 37 (17) (2012) 12714–12724.
- [25] G. Bahlakeh, et al., Molecular dynamics simulation study of proton diffusion in polymer electrolyte membranes based on sulfonated poly (ether ether ketone), *Int. J. Hydrogen Energy* 37 (13) (2012) 10256–10264.
- [26] G. Bahlakeh, M. Nikazar, M.M. Hasani-Sadrabadi, Understanding structure and transport characteristics in hydrated sulfonated poly (ether ether ketone)–sulfonated poly (ether sulfone) blend membranes using molecular dynamics simulations, *J. Membr. Sci.* 429 (2013) 384–395.
- [27] P. Chen, C. Chiu, C. Hong, Molecular analysis on methanol diffusion in a model nafion membrane, *J. Electrochem. Soc.* 155 (12) (2008) B1255–B1263.
- [28] S. Urata, et al., Molecular dynamics study of the methanol effect on the membrane morphology of perfluorosulfonic ionomers, *J. Phys. Chem. B* 109 (36) (2005) 17274–17280.
- [29] X. Ji, et al., Methanol distribution and electroosmotic drag in hydrated poly (perfluorosulfonic) acid membrane, *J. Phys. Chem. B* 112 (49) (2008) 15616–15627.
- [30] J. Pozuelo, et al., Molecular dynamics simulations of proton conduction in sulfonated poly (phenyl sulfone) s, *Macromolecules* 39 (25) (2006) 8862–8866.
- [31] Q.G. Zhang, et al., Microstructure dependent diffusion of water–ethanol in swollen poly (vinyl alcohol): a molecular dynamics simulation study, *Chem. Eng. Sci.* 64 (2) (2009) 334–340.
- [32] F. Khodaparast-Kazeroonian, S. Amjad-Iranagh, H. Modarress, Molecular dynamics simulation study of carboxylated and sulfonated poly (arylene ether sulfone) membranes for fuel cell applications, *Int. J. Hydrogen Energy* 40 (45) (2015) 15690–15703.
- [33] M. Saito, et al., Alcohol and proton transport in perfluorinated ionomer membranes for fuel cells, *J. Phys. Chem. B* 110 (48) (2006) 24410–24417.
- [34] G. Bahlakeh, et al., Investigation of the effects of methanol presence on characteristics of sulfonated aromatic electrolyte membranes: molecular dynamics simulations, *J. Power Sources* 243 (2013) 935–945.

- [35] H.S. Thiam, et al., Nafion/Pd–SiO₂ nanofiber composite membranes for direct methanol fuel cell applications, *Int. J. Hydrogen Energy* 38 (22) (2013) 9474–9483.
- [36] G.G. Kumar, et al., Fabrication and electro chemical properties of poly vinyl alcohol/para toluene sulfonic acid membranes for the applications of DMFC, *Solid State Ionics* 180 (2) (2009) 282–287.